Higher-order transverse modes of ultrashort isodiffracting pulses

Simin Feng* and Herbert G. Winful†
EECS Department, 1301 Beal Avene, University of Michigan, Ann Arbor, Michigan 48109-2122
(Received 14 July 2000; revised manuscript received 10 November 2000; published 20 March 2001)

We present a family of space-time nonseparable analytic solutions describing spatiotemporal dynamics of isodiffracting single-cycle and few-cycle pulses with Hermite–Gaussian and Laguerre–Gaussian transverse profiles. These solutions are space-time localized wave packets propagating in free space. The transverse field profile acts as a spatially dependent filter, modifying the pulse spectrum and removing certain frequencies. The consequences of those effects in the time domain are the distortions of pulse envelope and temporal wave form and the creation of ''dark pulses'' at certain transverse positions. In addition, due to the space-time coupling, the instantaneous transverse field pattern changes inside the pulse, as well as with propagation distance. These higher-order mode solutions can be used to analyze reflected or scattered terahertz pulses, and to understand the wave-form distortions of terahertz signals in applications. They are also capable of modeling pulsed fields of phase locking of both transverse and longitudinal modes in total mode-locked lasers.

DOI: 10.1103/PhysRevE.63.046602 PACS number(s): 42.25.Bs, 42.25.Fx, 42.65.Re, 41.20.Jb

I. INTRODUCTION

There is much current interest in the propagation of single-cycle and few-cycle ultrashort pulses in both the terahertz and optical regimes. On the theoretical front, several authors have discussed the propagation of ultrashort pulses using techniques that go beyond the slowly varying envelope approximation [1–6]. A key feature of these solutions is that the coupling between spatial and temporal variables leads to substantial pulse reshaping through diffraction even when such pulses propagate in free space. To data, however, most of the studies of single-cycle pulse propagation have considered only the fundamental Gaussian transverse mode. One notable exception is the work of Heyman and Beracha [7] in which a general exact solution is found for the higher-order Hermite–Gaussian transverse modes of a class of pulsed beams that have the property of being ''isodiffracting,'' i.e., all the frequency components in the pulse have the same Rayleigh range. Heyman and Beracha's focus in that paper was on the use of these solutions as an expansion basis for synthesizing the transient radiation from well-collimated apertures. Thus the detailed physical properties of these solutions for pulse spectra of interest in optics were not examined. In this paper we provide a thorough analysis of pulsed beams of higher-order transverse modes using spectra that are typically observed in terahertz experiments. These solutions are also relevant to recent experiments on the total mode locking of longitudinal and higher-order transverse modes in laser cavities [8,9]. In the terahertz regime, the advanced technology permits a measurement of the electric field of the terahertz pulse in both space and time [10]. This opens up the possibility of detection and experimental investigation of the transverse dynamic structure of ultrashort pulses in the single-cycle regime. An understanding of these higher-order single-cycle pulses helps one to analyze and understand temporal wave-form distortions of terahertz pulses upon reflection or scattering in many applications, such as T-ray imaging [11–13] and THz impulse ranging studies [14].

When the pulse width approaches the peak frequency, the effects of space-time coupling become significant. Space-time separable solutions cannot give a complete picture of the spatiotemporal dynamics of ultrashort pulses. In this work, we will present a family of space-time nonseparable exact solutions of the paraxial wave equation. These solutions contain single or few oscillations and are space-time localized wave packets with Hermite–Gaussian or Laguerre–Gaussian transverse profiles. The space-time coupling is an effect associated with the ultrawide bandwidth and the frequency-dependent spatial mode structure. It can be understood from modal structure dispersion: a spatial variation of the spatial mode structure with frequency. Unlike a monochromatic wave or a narrow-band pulse which is dominated by the characteristics of the carrier frequency, a single-cycle pulse contains contributions from all the frequency components within the full width at half maximum (FWHM) bandwidth. Hence the spatial variation of the spatial mode structure with frequencies leads to a space-time coupling in the time domain. As a result of the space-time coupling, we find that the instantaneous transverse profile of a pulse is a function of both the local time within the pulse and the propagation distance (or equivalently, the global time). In addition, whereas for monochromatic beams the electric field is strictly zero for all time at the nulls of the Hermite or Laguerre polynomials, the ''nulls'' of the pulsed beam have the nature of dark pulses or dark-ring pulses: a temporal hole in the bright background of the pulse envelope. We also find that the space-time coupling results in significant pulse reshaping and a strong dependence of the temporal pulse profiles on transverse coordinates.

II. DERIVATION OF HIGHER-ORDER ISODIFFRACTING PULSE SOLUTIONS

As an extension of our previous work [5], we start with the paraxial wave equation for the electric field:

*Present address: Lucent Technologies, Bell Labs Innovations, 101 Crawfords Corner Road, Holmdel, NJ 07733-3030. Electronic address: sfeng@engin.umich.edu
†Electronic address: winful@eecs.umich.edu

$$\left[\nabla_\perp^2 + 2ik\frac{\partial}{\partial z}\right]\tilde{U}(\mathbf{r},\omega)=0, \tag{2.1}$$

where $\nabla_\perp^2$ operates on the transverse coordinates and $k=\omega/c$. To form our particular pulsed beam solution, we use the broadband spectrum:

$$\tilde{S}(\omega)=(\omega\tau_0)^s\exp(-\omega\tau_0),\ \ (\omega\geqslant 0), \tag{2.2}$$

where $s\geqslant 1$ and $\tau_0>0$ are real parameters related to the bandwidth and the peak frequency ($\omega_p=s/\tau_0$) of the pulse. This set of spectra not only gives a closed-form analytic expression for the pulse temporal profile, but also describes quite well the spectra of single-cycle pulses in terahertz experiments [15–17].

The well-known Hermite–Gaussian beam solution of Eq. (2.1) is given by [18]

$$\tilde{H}_{mn}(\mathbf{r})=\frac{H_m(\xi)H_n(\eta)}{\sqrt{1+z^2/z_R^2}}\exp\left[\frac{ik\rho^2}{2R(z)}-\frac{\rho^2}{w^2(z)}-i\mathcal{G}_{mn}(z)\right], \tag{2.3}$$

where $H_m(\cdot)$ and $H_n(\cdot)$ are Hermite polynomials of order m and n. The arguments of the Hermite polynomials are normalized transverse coordinates:

$$\xi=\sqrt{2}\frac{x}{w(z)},\quad \eta=\sqrt{2}\frac{y}{w(z)}. \tag{2.4}$$

The beam size $w(z)$ and the radius of curvature of the wave front $R(z)$ are given by

$$w(z)=\sqrt{\frac{\lambda z_R}{\pi}\left(1+\frac{z^2}{z_R^2}\right)},\quad R(z)=z+\frac{z_R}{z}, \tag{2.5}$$

where z_R is the Rayleigh range of the beam. The Gouy shift $\mathcal{G}_{mn}(z)$ in Eq. (2.3) is given by

$$\mathcal{G}_{mn}(z)=(m+n+1)\arctan\left(\frac{z}{z_R}\right). \tag{2.6}$$

Note that we have neglected an unimportant constant in front of the expression Eq. (2.3), so $\tilde{H}_{mn}(\mathbf{r})$ is dimensionless. Multiplying Eq. (2.3) by the spectrum (2.2), we obtain

$$\tilde{U}_{mn}(\mathbf{r},\omega)=\frac{H_m(\xi)H_n(\eta)}{\sqrt{1+z^2/z_R^2}}(\omega\tau_0)^s \times\exp\left[-\omega\tau_0+\frac{ik\rho^2}{2R(z)}-\frac{\rho^2}{w^2(z)}-i\mathcal{G}_{mn}(z)\right]. \tag{2.7}$$

We are particularly interested in isodiffracting pulses, defined as pulses whose frequency components all have the same Rayleigh range [19]. This would be the case, for example, in an ideal mode-locked laser. By matching the curvature of wave fronts at the end mirrors of the cavity, all the frequency components inside the cavity are forced to have the same Rayleigh range which is determined by the cavity geometry. The Rayleigh range z_R in Eq. (2.7) is thus independent of frequency.

The time domain expression of the Hermite–Gaussian pulses can be obtained by taking the analytic inverse Fourier transform of Eq. (2.7) with respect to the local time $t'\equiv t-z/c$. The analytic inverse Fourier transform is defined by [20]

$$U_a(t)=\frac{1}{\pi}\int_0^\infty\tilde{U}(\omega)\exp(-i\omega t),\quad \mathrm{Im}\,t\leqslant 0, \tag{2.8}$$

where $\tilde{U}(\omega)$ is the spectrum of a real signal corresponding to the real part of the analytic signal $U_a(t)$. After the integration, we find that the space-time evolution of the isodiffracting Hermite–Gaussian pulses can be described by the compact expression:

$$U_{mn}(\mathbf{r},T)=\frac{\mathcal{H}_{mn}(\xi_T,\eta_T)}{\sqrt{1+z^2/z_R^2}}\frac{\exp[-i\mathcal{G}_{mn}(z)]}{(1+iT)^{s+1}\beta^{s+1}(\mathbf{r})}. \tag{2.9}$$

Here m and n are, respectively, x- and y-direction mode indices. The dimensionless local time $T(\mathbf{r},t)$ is given by

$$T(\mathbf{r},t)=\frac{t-\frac{1}{c}\left\{z+\frac{\rho^2}{2R(z)}\right\}}{\tau_0\beta(\mathbf{r})}, \tag{2.10}$$

where $\rho^2=x^2+y^2$. The quantity $\beta(\mathbf{r})$ is a transverse scaling parameter which scales the pulse width and bandwidth off axis [5]. It is given by

$$\beta(\mathbf{r})=1+\frac{\rho^2}{a^2(z)}, \tag{2.11}$$

where $a(z)$ is the transverse radius of the pulse. It has the same functional form as a monochromatic Gaussian beam:

$$a(z)=a_0\sqrt{1+\left(\frac{z}{z_R}\right)^2}, \tag{2.12}$$

where a_0 is the radius of the pulse at the focus and is related to the pulse width and the Rayleigh range through $a_0=\sqrt{2c\tau_0 z_R}$. The function $\mathcal{H}_{mn}(\cdot,\cdot)$ in Eq. (2.9) is a modified two-dimensional (2D) coupled Hermite polynomial, given by

$$\mathcal{H}_{mn}(x,y)=\sum_{k=0}^{[m/2]}\sum_{l=0}^{[n/2]}(-1)^{k+1} \times\frac{m!n!\Gamma[s+(m+n)/2-k-l+1]}{k!(m-2k)!l!(n-2l)!\Gamma(s+1)} \times(2x)^{m-2k}(2y)^{n-2l}, \tag{2.13}$$

where the gamma function $\Gamma[s+(m+n)/2-k-l+1]$ comes from the spectral integration of the 2D uncoupled Hermite polynomials $[H_m(x)H_n(y)]$. The gamma function $\Gamma(s+1)$ normalizes the fundamental Gaussian transverse

mode $\mathcal{H}_{00}(x,y)\equiv 1$. The arguments ξ_T and η_T in Eq. (2.9) are normalized time-coupled transverse spatial coordinates:

$$\xi_T = \sqrt{\frac{2}{\beta(\mathbf{r})(1+iT)}}\left[\frac{x}{a(z)}\right],$$
$$\eta_T = \sqrt{\frac{2}{\beta(\mathbf{r})(1+iT)}}\left[\frac{y}{a(z)}\right]. \tag{2.14}$$

Again, in Eq. (2.9) we neglected the unimportant constant in front of the expression to make it dimensionless for convenience. For certain values of m, n, and s, Eq. (2.9) becomes a multiple-valued function. In that case we only consider the principal value.

One unique feature of the isodiffracting Hermite–Gaussian pulses is that along hyperbolic trajectories of the Gaussian beam, their temporal and frequency information, such that the pulse shape (except for the Gouy shift), the spectrum, and the number of oscillations in the temporal wave form, remain invariant. This feature will be transparent if one replaces x and y by the relative coordinates u $(\equiv x/a(z))$ and $v(\equiv y/a(z))$ in Eqs. (2.9)–(2.14). Thus for any pair of fixed (u,v), except for the Gouy shift and the amplitude decay, the Hermite–Gaussian pulses are invariant along the trajectories:

$$x = u a_0 \sqrt{a+\frac{z^2}{z_R^2}}, \quad y = v a_0 \sqrt{1+\frac{z^2}{z_R^2}}. \tag{2.15}$$

For systems with cylindrical symmetry, the eigenmodes are Laguerre–Gaussian:

$$\tilde{L}_{pl}(\mathbf{r}) \propto \frac{w_0}{w(z)}\xi^{|l|}L_p^l(\xi^2)\exp\left[ik\frac{\rho^2}{2R(z)} - \frac{\rho^2}{w^2(z)}\right] \times \exp(il\phi - i\mathcal{G}_{pl}), \tag{2.16}$$

where $\rho^2 = x^2+y^2$ and ϕ is the azimuthal angle. Here p and l are transverse mode indices in the radial and azimuthal directions. The beam size $w(z)$ and radius of curvature $R(z)$ are given by Eq. (2.5). The Gouy shift $\mathcal{G}_{pl}(z)$ is given by

$$\mathcal{G}_{pl}(z) = (2p+|l|+1)\arctan\left(\frac{z}{z_R}\right). \tag{2.17}$$

The function $L_p^l(\cdot)$ in Eq. (2.16) is the Laguerre polynomial with an argument which is a square of the normalized transverse radius $\xi \equiv \sqrt{2}\rho/w(z)$. Following the same procedure, one obtains the Laguerre–Gaussian single-cycle pulses:

$$U_{pl}(\mathbf{r},T) = \frac{\xi_T^{|l|}\mathcal{L}_p^l(\xi_T^2)}{\sqrt{1+z^2/z_R^2}}\frac{\exp[il\phi - i\mathcal{G}_{pl}(z)]}{(1+iT)^{s+1}\beta^{s+1}(\mathbf{r})}, \tag{2.18}$$

where the definitions of T and $\beta(\mathbf{r})$ are the same as Eqs. (2.10) and (2.11), respectively. The function $\mathcal{L}_p^l(\cdot)$ in Eq. (2.18) is a modified Laguerre polynomial given by

$$\mathcal{L}_p^l(x) = \sum_{k=0}^{p}(-1)^k\binom{p+|l|}{p-k}\frac{\Gamma(s+k+|l|/2+1)}{\Gamma(s+1)}\frac{x^k}{k!}, \tag{2.19}$$

where the gamma function $\Gamma(s+k+|l|/2+1)$ comes from the spectral integration of the Laguerre polynomial. The gamma function $\Gamma(s+1)$ normalizes the fundamental Gaussian transverse mode $\mathcal{L}_0^0(x)\equiv 1$. The argument ξ_T in Eq. (2.18) is a time-coupled normalized transverse radius defined by

$$\xi_T \equiv \sqrt{\frac{2}{\beta(\mathbf{r})(1+iT)}}\frac{\rho}{a(z)}. \tag{2.20}$$

The unimportant constant coefficient in front of Eq. (2.18) is neglected and the function $U_{pl}(\mathbf{r},T)$ is dimensionless.

Equations (2.9) and (2.18) represent a family of single-cycle or few-cycle isodiffracting pulses of higher-order transverse modes without the slowly varying envelope approximation. They describe space-time localized wave packets propagating in free space. Notice that in Eqs. (2.9) and (2.18) the space and time variables are nonseparable. Such a coupling between space and time introduces some unique features which cannot be predicted from any space-time separable solutions or from monochromatic waves.

III. PHYSICAL PROPERTIES

In this section we will discuss general properties of these pulses. The particular form of the spectra does not affect the general properties significantly. What matters is the fact that the bandwidth and peak frequency of the pulse are comparable. In what follows we first clarify some of the quantities that characterize the pulse.

A. Field quantities

From Eqs. (2.9) and (2.18), the analytic field is a complex number which can always be written as a magnitude multiplied by an exponential phase. To simplify the expression, we rewrite them as

$$U_{ij}(\mathbf{r},T) = A_{ij}(\mathbf{r},T)\exp[-i\psi_{ij}(\mathbf{r},T) - i\mathcal{G}_{ij}(z)], \tag{3.1}$$

where ij represents mn for Hermite–Gaussian and pl for Laguerre–Gaussian. $A_{ij}(\mathbf{r},T)\geqslant 0$ is the magnitude and $\psi_{ij}(\mathbf{r},T)$ is the phase of the field excluding the Gouy phase. The total phase is

$$\Psi_{ij}(\mathbf{r},T) = -\psi_{ij}(\mathbf{r},T) - \mathcal{G}_{ij}(z). \tag{3.2}$$

The physical instantaneous electric field is given by the real part of Eq. (3.1):

$$E_{ij}(\mathbf{r},T) = A_{ij}(\mathbf{r},T)\cos[\psi_{ij}(\mathbf{r},T) + \mathcal{G}_{ij}(z)]. \tag{3.3}$$

In the figures that follow, we will plot some of the following quantities:

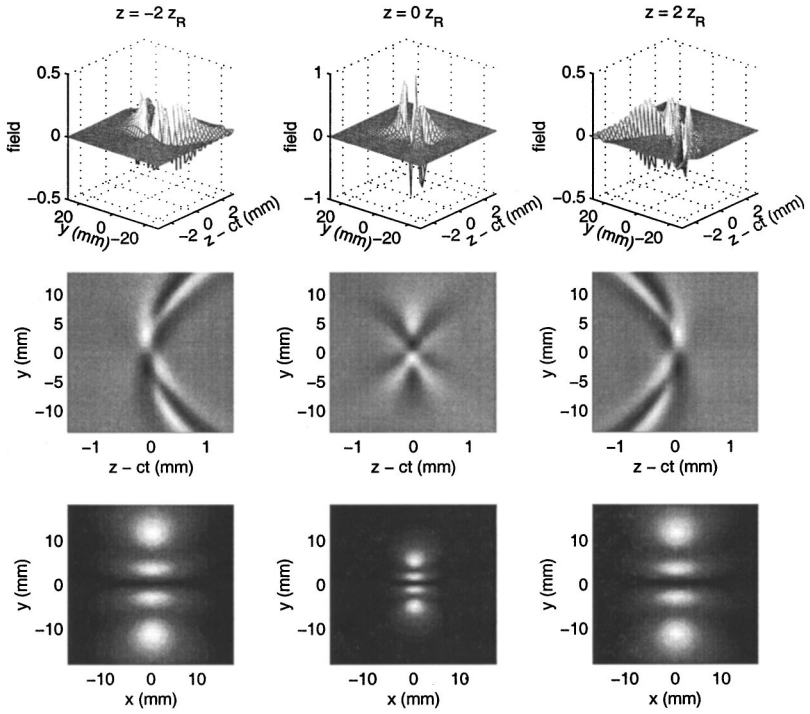

FIG. 1. Top row: spatiotemporal evolution of the electric field of a H_{03} single-cycle pulse. The pulse propagates from a plane ($z=-2z_R$) before the focus, at the focus ($z=0$), and to a plane ($z=2z_R$) after the focus. Center row: snapshots of the same field distribution in the plane $x=0$ at the corresponding propagation distances. Bottom row: time-integrated pulse intensity (energy density) at the corresponding planes.

field	$E_{ij}(\mathbf{r},T)$,
intensity	$[E_{ij}(\mathbf{r},T)]^2$,
time-integrated intensity	$\int_{-\infty}^{+\infty}[E_{ij}(\mathbf{r},T)]^2dt$,
phase of the field	$\Psi_{ij}(\mathbf{r},T)$,
ampltude of the field	$A_{ij}(\mathbf{r},T)$,
squared ampltude of the field	$[A_{ij}(\mathbf{r},T)]^2$.

Note that the time-integrated intensity is proportional to energy distribution in the transverse plane.

B. Spatiotemporal evolution

The transverse profiles of the pulses given by Eqs. (2.9) and (2.18) are on the average similar to the corresponding monochromatic higher-order modes. There are, however, a number of distinct features of these pulses that arise as a result of the space-time coupling implicit in Eqs. (2.14) and (2.20) and the frequency-dependency of transverse mode profiles.

To visualize these pulses we begin by plotting in Fig. 1 the spatiotemporal profile of the H_{03} pulse at three different propagation distances. The plane $z=0$ represents the focal plane where the waist of the pulsed beam is located (at $t=0$). The pulse converges towards this plane for $z<0$ and diverges towards infinity for $z>0$. The field along the y-direction exhibits oscillations as expected for the higher-order mode. The second row in the figure represents a lateral plot of the same field distribution where the bright regions have positive field strength and the dark regions are negative. While the top two rows in Fig. 1 show the instantaneous electric field, what is usually measured for optical frequency fields is the time-integrated intensity or the energy density distribution in a transverse plane. The bottom row in Fig. 1 shows the corresponding energy density. The transverse energy distribution of the pulsed beam H_{03} looks very much like that of the corresponding monochromatic beam, consisting of four bright spots along the y-direction with three dark regions or nulls in between. Upon closer inspection, however, it becomes clear that the minima of the pulsed beam contain finite energy whereas the minima of the monochromatic beam are strictly zero. Figure 2(a) shows the transverse-dependence of the energy density at the focus of the pulsed beam along the line $x=0$ while Fig. 2(b) shows a

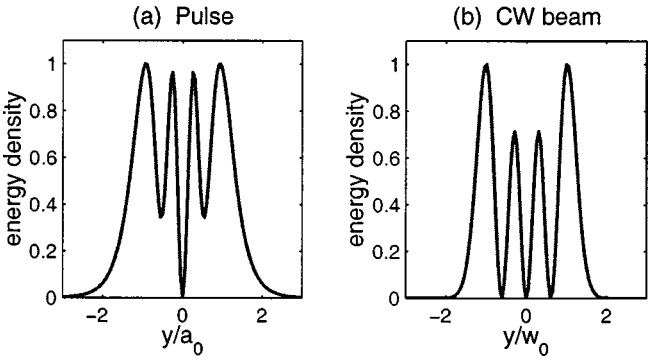

FIG. 2. y-dependence of the energy density in the focal plane along the line $x=0$. (a) for the H_{03} pulse, a_0 is the pulsed beam size at the focus. (b) For the monochromatic beam of the same Rayleigh range with the frequency at the peak of the pulse spectrum. w_0 is the beam waist of the monochromatic Gaussian beam.

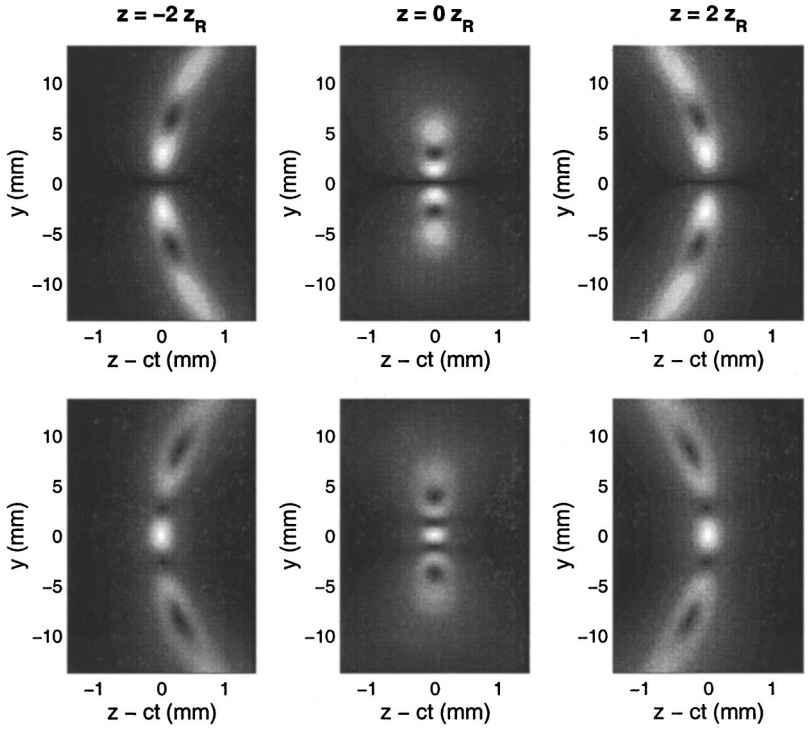

FIG. 3. Amplitude of the field in the plane $x=0$ at distances before the focus $z=-2z_R$, at the focus $z=0$, and after the focus $z=2z_R$. The top row is H_{03} mode while the bottom row is H_{04} mode. Except for the dark line on axis, the dark spots are the amplitude holes where the phase of the field is singular.

similar plot for a monochromatic beam of the same Rayleigh range whose frequency lies at the peak of the pulse spectrum. Except for diffraction, this transverse distribution is invariant during propagation. While the minima of the cw beam (the dark spots) have strictly zero energy, the minima of the pulsed beam contain as much as 40% of the energy at the maxima. Thus a certain amount of light is coupled into the center of the dark spots from the adjacent bright spots.

The reason for the finite energy at the nulls of the pulsed beams is the frequency-dependence of the zeroes of the Hermite polynomials. From the frequency domain representation in Eq. (2.7), it is seen that the pulsed H_{03} beam is made up of a distribution of different frequencies. Suppose a root of the function $H_3(\eta)$ is at $\eta\equiv\sqrt{2}y/w(z)=\eta_1$. Since w is a function of frequency, the location of the root along y will also depend on frequency. Thus in any transverse plane the roots of different frequency components do not necessarily overlap and hence the Fourier integral need not yield a zero at the minima of the transverse field distribution. We note that for odd modes symmetry requires the presence of a null at $x=0$ or $y=0$. This null is independent of frequency and hence the field on axis for the odd modes is strictly zero even for the pulsed beam.

Figures 3 compares the space-time amplitude distribution of the H_{03} and H_{04} pulsed beams in the $x=0$ plane at three propagation distances: before the focus ($z=-2z_R$), at the focus ($z=0$), and after the focus ($z=2z_R$). Here the dark regions have low field amplitude. The curvature of the space-time patterns follows $T(\mathbf{r},t)=0$ contour plots at the respective locations. Note that the H_{04}, an even mode, has a bright spot on axis.

C. Phase singularities

The concept of phase singularities in wave fronts was first introduced by Nye and Berry [21]. Phase singularities are spatial points where the amplitude of the electric field is zero and hence the phase of the field is indeterminate. Associated with the amplitude holes in Fig. 3 are phase singularities. Figure 4 shows the contour plot of the phase of the field of the H_{04} pulse in the plane $x=0$ at the time $t=0$ (at the focus). At the positions of the four dark spots corresponding to those in the bottom plots of Fig. 3, the phase can be any value (singular). The thick curves in Fig. 4 represent the singular curves along which the amplitude of the field is zero and the phase is indeterminate (any value). The phase singular curves are associated with the complex roots whose real parts equal the values of y on the singular curves.

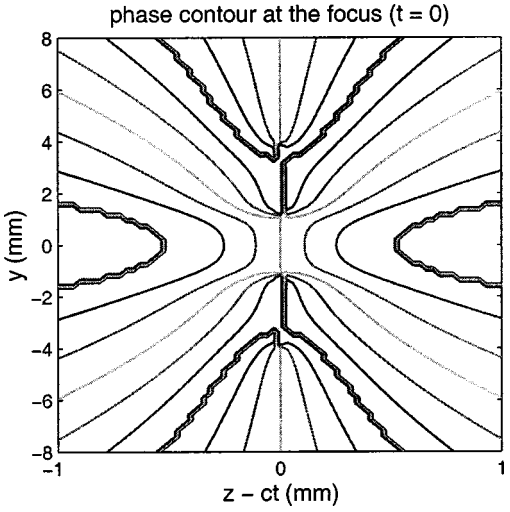

FIG. 4. Contour plot of the phase of the field in the plane $x=0$ at the time $t=0$ (at the focus) for the H_{04} pulse. At the dark spots (amplitude holes) corresponding to those in the bottom plots of Figs. 3 are the phase singularities. The thick curves represent the phase singular curves along which the phase is indeterminate.

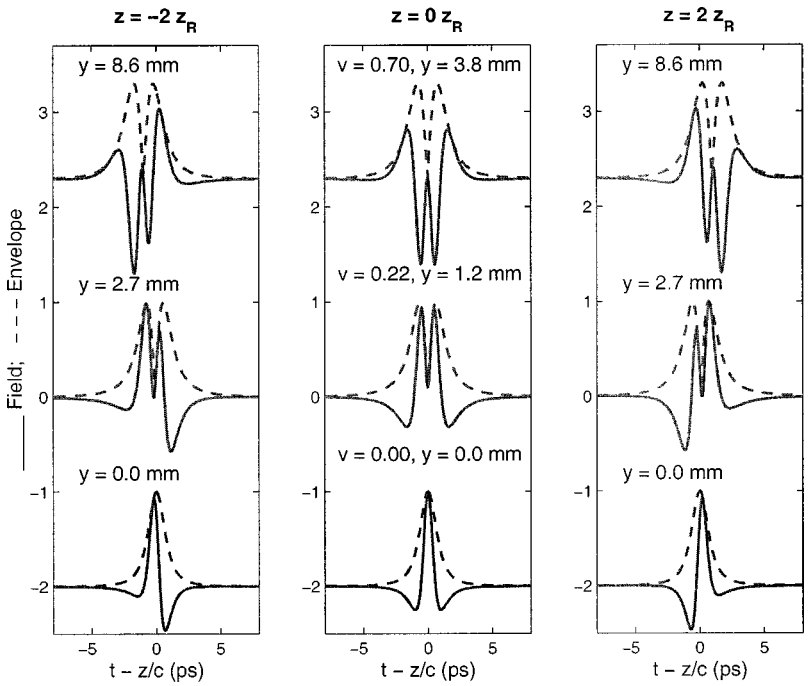

FIG. 5. Amplitudes (dashed lines) and electric fields (solid lines) of the H_{04} pulse on axis ($v=0.00$) and along two hyperbolic trajectories through the center of the two dark spots ($v=0.22$ and 0.70). The corresponding real positions are given in y. A temporal hole appears in the center of the amplitudes at the positions of the nulls, resulting in dark pulses. The electric fields of the dark pulses have dramatic distortion.

In the single-cycle regime the phase singularity can be directly reflected in the temporal profile of the pulse. It should be possible to observe wave-form distortion due to the phase singularity in phase sensitive experiments such as terahertz imaging and impulse scattering. They are recognizable features in the temporal wave forms of single-cycle pulses and could be used as indications of certain properties of targets [21]. Analysis of the temporal profiles of single-cycle pulses in the presence of the phase singularities is helpful to understand some general features in the wave-form distortions of terahertz signals in applications.

D. Dark pulses

As already noted, the electric field does not necessarily vanish for all time at the ''nulls'' of the pulsed beams. The pulse shapes measured at these ''nulls'' have the nature of dark pulses, with a temporal hole in the bright background of the amplitude of the field. Figure 5 shows the amplitudes (dashed lines) and electric fields (solid lines) of the H_{04} pulse on axis ($v=0.00$) and along two hyperbolic trajectories through the centers of the two dark spots ($v=0.22$ and 0.70). A temporal hole appears in the center of the amplitude at the positions of the two nulls. The depth of the hole depends on the distance to the center of the dark spot. The existence of the temporal hole can be seen in the space-time coupling in Eqs. (2.13) and (2.14). Corresponding to each real root (ξ_1,η_1) of the function $\mathcal{H}_{mn}(\cdot,\cdot)$, there are real solutions (x,y,z)'s only when $T(\mathbf{r},t)=0$, and no real solution when $T(\mathbf{r},t)\neq 0$. This causes the temporal hole to appear in the center $[T(\mathbf{r},t)=0]$ of the amplitude. The amplitude hole and phase singularity cause a dramatic distortion in the electric fields of the dark pulses as shown by the solid lines in plots.

The temporal hole is due to zero-crossing dispersion of Hermite polynomials. The peak of the amplitude is located at the space-time position where all the frequencies are in phase. Depending on the transverse position, the frequency components of the pulse are either in phase or π out of phase. The frequency-dependent zeroes of the Hermite polynomials introduce π-phase shifts between frequencies and hence bring down the peak of the amplitude, resulting in the dark spots in Fig. 3. At the centers of the dark spots the temporal hole dips down to zero since almost half frequency components are out of phase with the other half.

E. Spectrum reshaping

Equation (2.7) implies that the Hermite polynomial acts as a spatially dependent filter which modifies the spectrum of the fundamental pulse, removes certain frequencies at the nulls of the Hermite polynomial, and introduces a π-phase shift between frequency components. These filter effects are demonstrated in Fig. 6 which shows the amplitude spectra at $x=0$ and several relative coordinates $v(\equiv y/a(z))$ for the H_{04} pulse. The spectra are invariant along the hyperbolic rays of the Gaussian beam. The zeroes in the off-axis spectra ($v\neq 0$) are located at the zeroes of the Hermite polynomial taken as a function of frequency. There is a π-phase shift between the frequency components on the left and right of the zero transmission point. The dashed vertical line marks the position of the central frequency which is defined as the center of gravity of the spectrum:

$$\omega_c \equiv \frac{\int_0^\infty \omega |\tilde{E}(\omega)|^2 d\omega}{\int_0^\infty |\tilde{E}(\omega)|^2 d\omega}. \tag{3.4}$$

In the plots at the two dark spots ($v=0.22$ and 0.70), the removed frequency is very close to the central frequency. Thus almost half of the frequency components are π out of phase with the other half, resulting in the deepest hole (zero) in the peak of the amplitude. The zero transmission point in

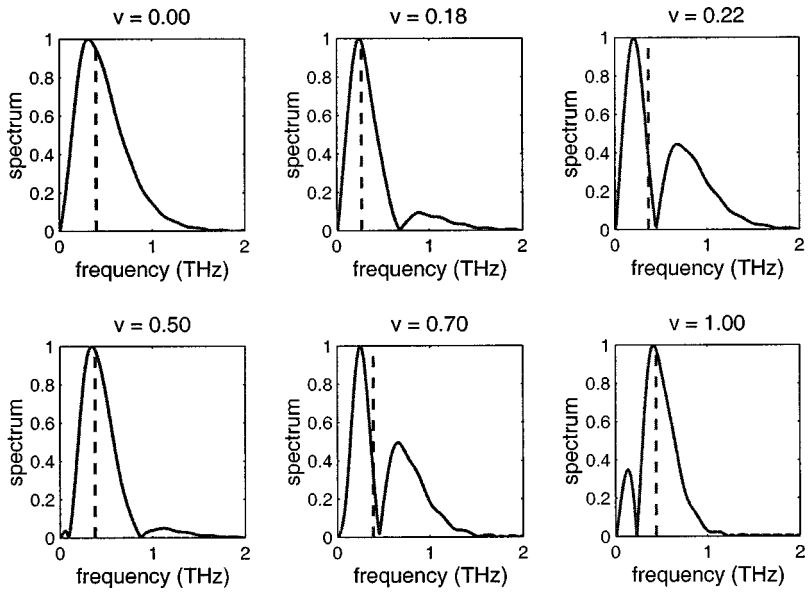

FIG. 6. Filter effect of the transverse profile which modifies the spectrum and removes certain frequencies, plotted for the spectra of the H_{04} pulse at the $x=0$ along several hyperbolic rays of the Gaussian beams given by v. The dashed vertical line in each plot indicates the position of the carrier frequency.

the plots shifts to the red end of the spectrum as one moves outwards crossing each root of the Hermite polynomial due to the larger beam size of the lower frequency.

F. Dynamics of electric fields

Another effect of the space-time coupling is the time-dependence of the transverse pattern of the electric field. The transverse pattern is a function of both local time and propagation distance z (or equivalently global time). The evolution of the electric field of a H_{12} pulse on transverse planes is shown in Fig. 7. The plots in the same row represent the field at different local times but the same distance, while the plots in the same column show the field at different distances but the same local time. Along the rows, one observes the inner dynamic structure of the pulse, i.e., snap shots inside the pulse at the same distance. Along the columns, one observes the propagation dynamics at the same position relative to the pulse center. Since the temporal and transverse coordinates are coupled, the field transverse pattern changes with both local and global times. Figure 8 shows the transverse patterns of the field of a L_0^3 pulse at the corresponding planes in

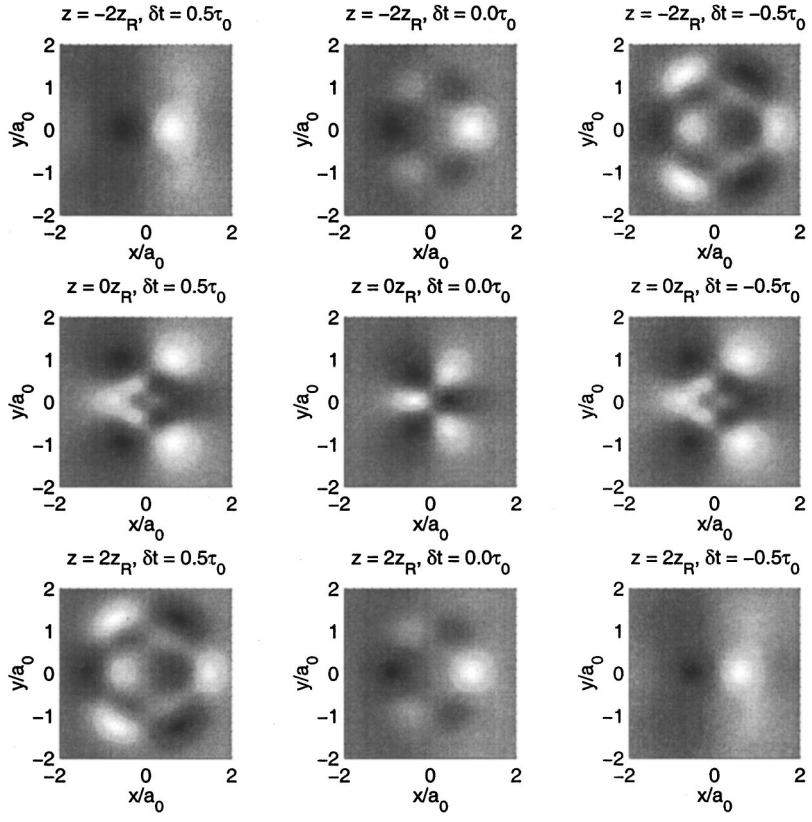

FIG. 7. Spatiotemporal dynamics of transverse patterns of the electric field of a H_{12} pulse. The plots in the same row show the electric field in the transverse planes at the same propagation distance (global time), but different relative positions (represented by δt) to the pulse center. The plots in the same column show the electric field at different propagation distances, but the same relative position. The transverse coordinates are normalized by the beam size (a_0) at the focus.

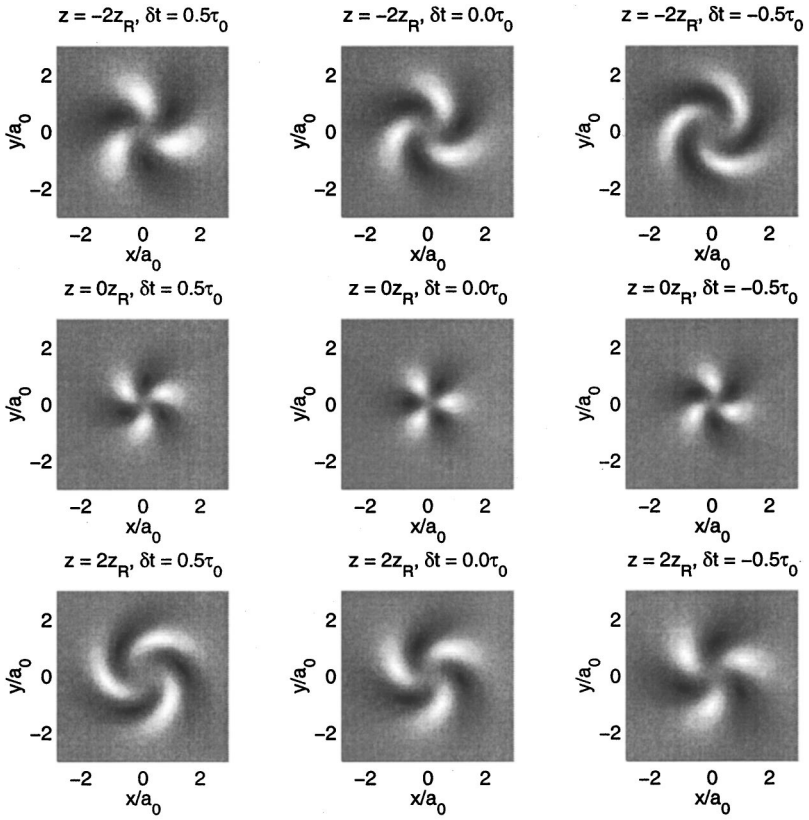

FIG. 8. Spatiotemporal dynamics of transverse patterns of the electric field of a L_0^3 pulse at the corresponding planes in Fig. 7.

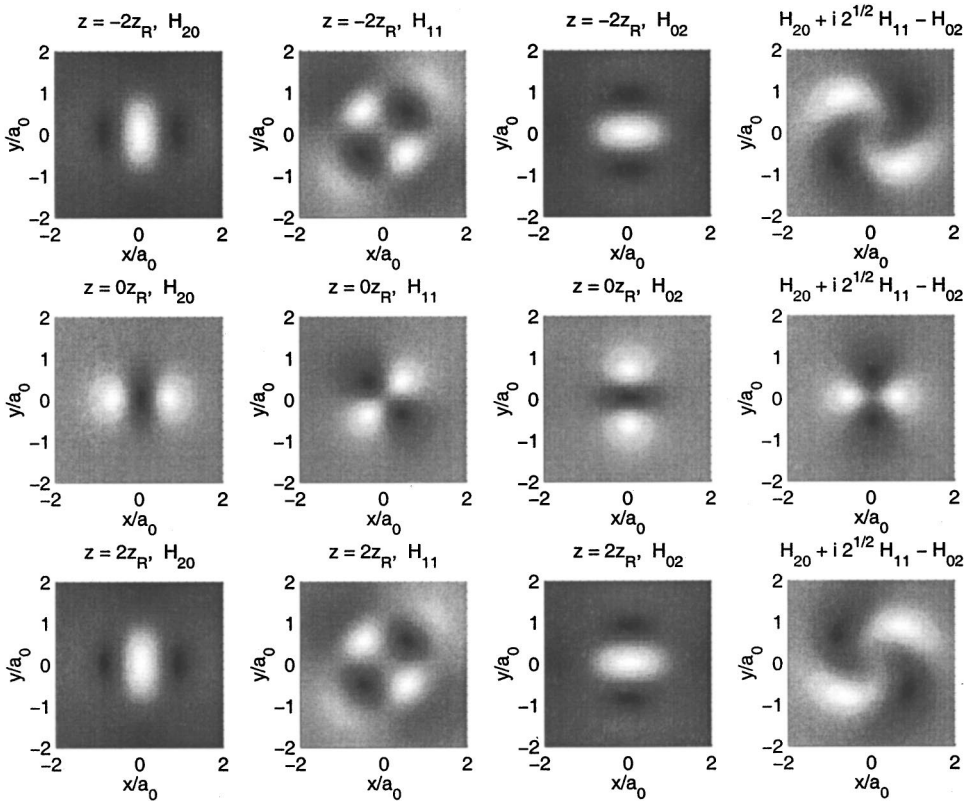

FIG. 9. Mode transformation between Hermite–Gaussian and Laguerre–Gaussian single-cycle pulses. With a proper phase relationship, three Hermite–Gaussian pulses (H_{20}, H_{11}, and H_{02}) are converted into a Laguerre–Gaussian pulse (L_0^2). The electric fields are plotted in the transverse planes through the pulse center ($t=z/c$) at several propagation distances.

Fig. 7. The rotation is due to the azimuthal dependence of the phase of the field in the Laguerre–Gaussian transverse profile.

G. Mode transformation

The transformation between monochromatic Hermite– and Laguerre–Gaussian modes [22] also holds for the pulsed beams. This can be shown by multiplying the original transformation formula by the pulse spectrum and taking an analytic inverse Fourier transform. A transformation of three Hermite–Gaussian pulses of H_{20}, H_{11}, and H_{02} into a Laguerre–Gaussian pulse of L_0^2 is shown in Fig. 9 for several propagation distances. The fields are plotted in the transverse planes through the pulse center $(t=z/c)$ for all the distances.

IV. SUMMARY

We have presented a family of space-time nonseparable solutions of isodiffracting single-cycle and few-cycle pulses of higher-order transverse modes. The space-time coupling is a consequence of the modal structure dispersion. Similar to the group velocity dispersion which causes a temporal waveform distortion, the modal structure dispersion results in the temporal distortion as well. Due to the space-time coupling, a certain amount of light is coupled into the dark regions of the transverse profiles, resulting in dark pulses, and the transverse pattern of the field changes upon propagation. Owing to the isodiffracting nature, these solutions can be used to study the pulsed fields of phase locking of both transverse and longitudinal modes in total mode-locked lasers. Since Hermite–Gaussian and Laguerre–Gaussian beams form complete sets of basis functions for any two-dimentional space, the pulses presented here can be used to analyze reflected and scattered terahertz signals.

ACKNOWLEDGMENT

This work is partially supported by the National Science Foundation through the Center for Ultrafast Optical Science under STC PHY 8920108.

[1] R. W. Ziolkowski and J. B. Judkins, J. Opt. Soc. Am. A **9**, 2021 (1992).
[2] D. You and P. H. Bucksbaum, J. Opt. Soc. Am. B **14**, 1651 (1997).
[3] A. E. Kaplan, J. Opt. Soc. Am. B **15**, 951 (1998).
[4] M. A. Porras, Phys. Rev. E **58**, 1086 (1998).
[5] S. Feng and H. G. Winful, Phys. Rev. E **61**, 862 (2000).
[6] G. C. Sherman, J. Opt. Soc. Am. A **6**, 1382 (1989).
[7] E. Heyman and I. Beracha, J. Opt. Soc. Am. A **9**, 1779 (1992).
[8] D. Côté and H. M. van Driel, Opt. Lett. **23**, 715 (1998).
[9] S. R. Bolton, R. A. Jenks, C. N. Elkinton, and G. Sucha, J. Opt. Soc. Am. B **16**, 339 (1999).
[10] Z. Jiang and X.-C. Zhang, Opt. Lett. **23**, 1114 (1998).
[11] B. B. Hu and M. C. Nuss, Opt. Lett. **20**, 1716 (1995).
[12] D. M. Mittleman, R. H. Jacobsen, and M. C. Nuss, IEEE J. Sel. Top. Quantum Electron. **2**, 679 (1996).
[13] D. M. Mittleman, S. Hunsche, L. Boivin, and M. C. Nuss, Opt. Lett. **22**, 904 (1997).
[14] R. A. Cheville and D. Grischkowsky, Appl. Phys. Lett. **67**, 1960 (1995).
[15] Ch. Fattinger and D. Grischkowsky, Appl. Phys. Lett. **54**, 490 (1989).
[16] L. Xu, X.-C. Zhang, D. H. Auston, and B. Jalali, Appl. Phys. Lett. **59**, 3357 (1991).
[17] P. Uhd Jepsen and S. R. Keiding, Opt. Lett. **20**, 807 (1995).
[18] A. E. Siegman, *Lasers* (University Science, Sausalito, 1986).
[19] E. Heyman and T. Melamed, IEEE Trans. Antennas Propag. **AP-42**, 518 (1994).
[20] M. Born and E. Wolf, *Principles of Optics*, 6th ed. (Cambridge University Press, Cambridge, England, 1998).
[21] J. F. Nye and M. V. Berry, Proc. R. Soc. London, Ser. A **336**, 165 (1974).
[22] M. W. Beijersbergen, L. Allen, H. E. L. O. van der Veen, and J. P. Woerdman, Opt. Commun. **96**, 123 (1993).